

Brown Carbon Production in Ammonium- or Amine-Containing Aerosol Particles by Reactive Uptake of Methylglyoxal and Photolytic Cloud Cycling

David O. De Haan,^{*,†} Lelia N. Hawkins,[‡] Hannah G. Welsh,[‡] Raunak Pednekar,[‡] Jason R. Casar,[‡] Elyse A. Pennington,[‡] Alexia de Loera,[†] Natalie G. Jimenez,[†] Michael A. Symons,[†] Melanie Zauscher,[†] Aki Pajunoja,[§] Lorenzo Caponi,^{||,⊥} Mathieu Cazaunau,^{||} Paola Formenti,^{||} Aline Gratien,^{||} Edouard Pangui,^{||} and Jean-François Doussin^{||}

[†]Department of Chemistry and Biochemistry, University of San Diego, 5998 Alcalá Park, San Diego, California 92110, United States

[‡]Department of Chemistry, Harvey Mudd College, 301 Platt Blvd, Claremont, California 91711, United States

[§]Department of Applied Physics, University of Eastern Finland, P.O. Box 1627, 70211 Kuopio, Finland

^{||}Laboratoire Interuniversitaire des Systèmes Atmosphériques (LISA), UMR7583, CNRS, Université Paris-Est-Créteil (UPEC) et Université Paris Diderot (UPD), Institut Pierre Simon Laplace (IPSL), 94010 Créteil, France

Supporting Information

ABSTRACT: The effects of methylglyoxal uptake on the physical and optical properties of aerosol containing amines or ammonium sulfate were determined before and after cloud processing in a temperature- and RH-controlled chamber. The formation of brown carbon was observed upon methylglyoxal addition, detected as an increase in water-soluble organic carbon mass absorption coefficients below 370 nm and as a drop in single-scattering albedo at 450 nm. The imaginary refractive index component k_{450} reached a maximum value of 0.03 ± 0.009 with aqueous glycine aerosol particles. Browning of solid particles occurred at rates limited by chamber mixing (<1 min), and in liquid particles occurred more gradually, but in all cases occurred much more rapidly than in bulk aqueous studies. Further browning in AS and methylammonium sulfate seeds was triggered by cloud events with chamber lights on, suggesting photosensitized brown carbon formation. Despite these changes in optical aerosol characteristics, increases in dried aerosol mass were rarely observed ($<1 \mu\text{g}/\text{m}^3$ in all cases), consistent with previous experiments on methylglyoxal. Under dry, particle-free conditions, methylglyoxal reacted (presumably on chamber walls) with methylamine with a rate constant $k = (9 \pm 2) \times 10^{-17} \text{ cm}^3 \text{ molecule}^{-1} \text{ s}^{-1}$ at 294 K and activation energy $E_a = 64 \pm 37 \text{ kJ/mol}$.



INTRODUCTION

Atmospheric aerosol particles have a strong direct effect on climate through scattering and absorption of light and contribute greatly to uncertainty in climate predictions. It is therefore critical to measure the optical properties of typical atmospheric aerosol, but for secondary organic aerosol (SOA), there is no “typical” particle. SOA forms and evolves as compounds partition back and forth between the gas and particle phase.¹ However, reversible chemical reactions have caused the gas/particle equilibria of some individual compounds, particularly aldehydes, to favor the particle phase by $>10\times$ beyond theoretical predictions.^{2,3} Aldehydes have also been implicated in the aqueous-phase formation of high molecular weight oligomers⁴ and light-absorbing compounds known as brown carbon⁵ or humic-like substances (HULIS).^{6–11} While most brown carbon in the atmosphere is primary, emitted during combustion of biomass and other fuels, 30% of brown carbon¹²—and likely all the oligomers¹³—

are produced in the atmosphere. It is generally believed that condensed-phase processes, either in the aqueous or organic aerosol phase, are responsible for secondary production of oligomers and brown carbon species.^{14–18}

It has recently been shown that aqueous phase Maillard reactions between aldehyde and amine compounds generate products that are physically and chemically similar to aqueous extracts of atmospheric organic aerosol material, but with lower N/C ratios.¹⁹ The initial steps of these reactions, while quite slow in bulk phase studies, have been shown to be much faster in evaporating aerosol particles.²⁰ The Maillard reactions also produce light-absorbing and oligomeric products,^{21–24} but these processes have rarely been studied in aerosol-phase

Received: January 9, 2017

Revised: May 15, 2017

Accepted: May 31, 2017

Published: May 31, 2017

experiments. Here, we report chamber measurements of browning in aerosol containing ammonium sulfate (AS) or amines that occurs on a time scale of minutes upon the addition of methylglyoxal gas and after cloud cycling with solar simulator lights.

METHODS

The Chamber for Experimental Multiphase Atmospheric Simulation (CESAM) at LISA is a 4.2 m³ evacuable, stirred, temperature- and pressure-controlled cylindrical stainless steel chamber with solar simulator lights monitored by temperature, pressure, and flow sensors, as described in ref 25. Gas fills were completed using high-purity oxygen tanks and boil-off from a liquid nitrogen tank at an 80:20 v/v ratio. Gas phase contents were monitored by RH, ozone, and NO_x sensors, along with proton transfer reaction mass spectrometry (PTR-MS, KORE Technology, Series II, data corrected by dividing by the sum of water cluster signals at *m/z* 21 and 39). AS, methylammonium sulfate (pH 4), or glycine particles were atomized (TSI constant-output atomizer) from 1, 2, or 10 mM solutions, respectively. Unless otherwise stated, aerosol flows were diffusion dried to <5% relative humidity (RH) before introduction into the chamber. Particle and droplet size distributions were measured by scanning mobility particle sizing (SMPS, TSI 3080/3772, 20–900 nm, sampling from the central volume of the chamber via 1 m Nafion drying tube) and scattering spectrometer (Welas, Palas Particle Tech., 0.5 to 15 μm, sampling at 2 L/min from flange of chamber), respectively. The extinction and scattering of dried particles from the chamber were measured by cavity attenuated phase shift spectrometers (Aerodyne CAPS-PM single scattering albedo²⁶ and -PMex, 0.85 LPM sampling rates) at 450 and 630 nm, respectively, via Nafion drying tube, with instruments baselined by zeroing extinction and scattering signals on filtered sample flows at least every 15 min to remove any signals from gas-phase absorbers. Extinction and scattering data were normalized by dry SMPS mass, assuming density = 1 g cm⁻³ (as discussed in the Supporting Information). SMPS number concentration and mass were then corrected for dilution caused by flows into the chamber, which keep the chamber just above atmospheric pressure.

In order to estimate the complex index of refraction, uncorrected number concentrations were used to simulate uncorrected CAPS measurements of extinction and scattering at 450 nm. Measurements were averaged at 135 s time resolution. The mie_single.pro routine²⁷ was used to perform optical calculations of extinction and scattering assuming homogeneous spherical particles. The real component (*n*) of the refractive index was varied without any *a priori* information between 1.33 and 2.0 in steps of 0.01, and the imaginary component *k* between 0 (no absorption) and 0.05 in steps of 0.001, such that all possible combinations within these ranges were tested. Reported complex refractive indexes correspond to averages of the values for which differences between calculated and measured extinction and scattering values were both below measurement error (<5%).

Methylglyoxal gas was generated by heating viscous, concentrated methylglyoxal solutions into evacuated bulbs, the contents of which were flushed into the chamber with a N₂ flow. The viscous methylglyoxal solutions were produced by repeated pumping on 40% w/w methylglyoxal solutions (Alfa-Aesar) interspersed with disrupting the solid surface films that formed. Methylglyoxal concentrations were calibrated using an

FTIR integrated band intensity of 6.3 × 10⁻¹⁸ cm molecule⁻¹ cm³ from 2720 to 2940 cm⁻¹ (EUROCHAMP database).²⁸ Pure methylamine gas (Fluka, > 99%) was added by syringe injection through a septum into a flow of N₂ into the chamber. The chamber was humidified by step additions of ultrapure water vapor from a pressurized steel vessel. Water was purified to >18.2 MΩ in a reverse osmosis system (Elga Stat Maxima), which also includes microfiltration, nuclear-grade deionization, and activated carbon and 254 nm irradiation modules. Elevated RH in the humidified chamber was maintained by routing incoming N₂ and O₂ through a temperature-controlled bubbler containing ultrapure water.

Particle phase state and phase transitions over RH were monitored in some experiments by an Aerosol Bounce Instrument (ABI, see ref 29). Briefly, ABI measures the mechanical bounce of diffusion-dried, size-selected (Vienna-type DMA, open loop configuration, N₂ sheath gas), and then humidified (Nafion multitube) aerosols bounced from a MOUDI single-stage impactor plate. The corrected bounced fraction (BF; bounced-to-total particle number ratio, measured with two CPCs, TSI 3010) has a well-known relationship with the phase state of the amorphous SOA particles. A typical bounce curve of solid/semisolid SOA particles is an inverse sigmoid-curve along RH where BF drops from ~0.8 to 0 as particles undergo phase transition from semisolid to fully liquid.²⁹ ABI was tested with ammonium sulfate and sucrose particles multiple times during the campaign. In addition, nebulized methylglyoxal solutions were measured prior to the campaign. The polished aluminum MOUDI impactor plate cover was replaced for every RH scan to prevent particles attached to the plate from suppressing subsequent BF values. In normal mode, ABI scanned RH from ~10% to ~85% in 1 h. In some cases, the relative change in BF was monitored at a fixed RH.

In select experiments, a particle-into-liquid sampler (PILS) collected particles from the central volume of the chamber. The UV/visible absorbance of its aqueous effluent (0.5 mL min⁻¹) was analyzed online by a liquid waveguide capillary cell (LWCC-3100) with a 0.94-m optical path length coupled to a UV/vis spectrometer (Ocean Optics DT-Mini-2 lamp, USB-4000 detector) as in refs 12, 30, and 31. The PILS sampled ~6 LPM from the chamber (plus ~10 LPM makeup dry N₂, both flows were continuously recorded) in order to minimize chamber dilution. PILS-based mass absorption coefficients (MAC) at 1 min resolution were determined using SMPS integrated aerosol mass (eq 1).

$$\text{MAC (cm}^2 \text{ g}^{-1}\text{)} = \frac{[\text{Abs}_e(365 \text{ nm}) - \text{Abs}_e(550 \text{ nm})]}{bC \left(\frac{V_{\text{sampled}}}{V_{\text{output}}} \right)} \quad (1)$$

where Abs_e(λ) is ln-based absorbance at a given wavelength, *b* = 94 cm path length, *C* is total SMPS aerosol concentration in g/L (assuming particle density = 1 g/cm³), *V*_{sampled} is PILS air sampling rate (~6 L/min), and *V*_{output} is PILS liquid outflow rate (mL/min). MAC(λ) was averaged across a 10 nm range and referenced to baseline signals at 550 nm (also using a 10 nm window). This differs from previous brown carbon characterization using similar equipment where 700 nm was identified as a good reference wavelength.^{12,30,31} However, in this study, lamp drift at 700 nm was found to be greater than at 550 nm. The tail of brown carbon absorbance does not extend to 550 nm in our measurements. However, should any small

Table 1. List of Methylglyoxal Gas Addition Experiments^a

expt #	[MeGly] ^b (ppm)	aerosol type	aerosol conc. ($\mu\text{g}/\text{m}^3$)	RH at MeGly addition (%)	mass increase ($\mu\text{g}/\text{m}^3$)	illum. time (h)	albedo change (rapid ^c)	albedo change (total)	k_{max}	index of refraction, imaginary ^d
1	0.75	AS	13	<5%	+1	0	-0.038	-0.025		0.016 ± 0.005
2	0.80	AS	18	<5%	<0.2	2.5	-0.023	-0.054		0.014 ± 0.005
3	1.8	AS	32	<5%	<1	0	-0.019	-0.032 ^e		0.013 ± 0.007
4	6.9 ^f	Glycine	74	69%	<3	1.7	-0.012	-0.049		0.030 ± 0.009
5	3.6 ^f	MeAS	73	71%	<1	1.9	-0.008	-0.041		0.008 ± 0.005
6	2.7	no seeds	<0.05	<5%	0.6	1.6	n/a	n/a		n/a

^aNotes: MeAS = methylammonium sulfate. ^bTabulated methylglyoxal (MeGly) concentrations are the highest values measured by PTR-MS. ^cOccurring within 5 min of MeGly addition. ^dCorrected for truncation but not any nonlinearity or intercept in the relationship between scattering and extinction. ^eUntil 1st cloud event; aerosol not dried before sampling by CAPS. ^f[MeGly] was 1.0 ppm prior to gas phase addition due to equilibration from the walls of the humidified chamber.

absorbance occur at 550 nm, this correction would produce a small underestimate of aerosol extract absorptivity. Any spectra impacted by air bubbles generated in the PILS were omitted from the time series.

RESULTS

Chamber experiments are listed in Table 1.

Ammonium Sulfate Aerosol Seeds. Conditions, dilution-corrected PTR-MS and SMPS data sets, and mass-normalized CAPS extinction, scattering, and albedo are shown in Figures S1, 1/S2, and S3 for experiments 1, 2, and 3, respectively. In these experiments, dry AS aerosol was exposed to methylglyoxal gas, water vapor, methylamine gas, and cloud events. Although the CAPS instrument was calibrated with AS aerosol immediately prior to each experiment, after the AS aerosol injection was completed in each experiment the single-scattering albedo was stable at a value between 0.96 and 0.99, rather than 1. The reason for this discrepancy is a slight nonlinearity in the scattering vs extinction measurements as a function of particle loading (see Figure S4 and discussion in the Supporting Information), which causes measured albedo to decline slightly as particle loadings decrease, even during AS control experiments (Figure S5). For this reason, we focus here on observed departures from this declining baseline.

Sudden drops in single-scattering albedo were observed whenever methylglyoxal gas was added to the dry chamber containing crystalline AS particles (Figures S1, 1/S2, S3). These albedo drops of 0.02 to 0.04 occurred in less than 1 min (the chamber mixing time), indicating a very rapid process, and yet were accompanied by negligible aerosol growth (<1 $\mu\text{g}/\text{m}^3$). These observations suggest a limited, reactive uptake of methylglyoxal onto crystalline AS aerosol particles, causing the formation of strongly light-absorbing products at the aerosol surface.

Water vapor was added next in experiments 1 and 2, bringing the chamber from an essentially dry state to 60% or 88% RH, respectively, and causing a number of changes to be observed in the dried aerosol (sampled by CAPS and SMPS through a Nafion dryer). First, the mass-normalized scattering of the aerosol particles increased by a factor of ~ 2 within 2 min at both 450 and 650 nm, indicative of shape changes induced by water uptake, even in experiment 1 where RH remained below the deliquescence point.³² Second, the PTR-MS data show that chamber humidification triggers a 40 to 60% increase in the water-corrected signal for methylglyoxal gas over a ~ 6 min period. (The water-corrected signal is the ratio $[m/z 73]/[m/z 21 + m/z 39]$, which for compounds such as methylglyoxal with proton affinities close to water, normally decreases when RH

rises.³³) Third, in the 20–30 min after water addition, the aerosol single-scattering albedo increases by 0.027 and 0.010, respectively, in experiments 1 and 2. Finally, the dilution-corrected dry SMPS mass decreases over 15 min by 1.3 to 2.8 $\mu\text{g}/\text{m}^3$ upon water addition, more than offsetting any earlier growth. This loss of aerosol-phase brown carbon and mass, combined with the return of methylglyoxal to the gas phase, suggests that the uptake of water causes hydrolysis of the brown carbon products formed earlier under dry conditions and allows methylglyoxal to re-equilibrate between the aerosol and gas phase. These observations are consistent with the hydrolytic destruction of at least 70% of the brown carbon products at 60% RH, and the loss of all brown carbon products at 88% RH. Clearly, the dry browning process triggered by methylglyoxal uptake onto AS seeds is largely reversible upon humidification.

The addition of 2 ppm methylamine gas at $t = 4:22$ h is labeled in Figure 1 ($t = 4$ h in Figure S1 and $t = 4:50$ h in Figure S3). While methylamine addition caused little change in aerosol optical or physical properties in humidified experiments 1 and 2, significant changes were seen in the gas phase. Obviously, the methylamine PTR-MS signal increased, but unlike methylglyoxal (whose PTR-MS signal took less than 2 min to reach a maximum after its gas phase addition), methylamine gas concentrations increased for >20 min, likely due to “stickiness” on steel surfaces in the chamber or sampling line. At the same time, methylglyoxal gas concentrations dropped by 50% in the 45 min after methylamine addition in both humidified experiments 1 and 2, and by 78% under dry conditions in experiment 3. Over the same period, the PTR-MS signal for the imine product of the reaction of methylglyoxal and methylamine, $\text{CH}_3\text{C}(\text{O})\text{CH}=\text{NCH}_3$ observable at $m/z = 86$, increases by a factor of 2 or more. The $\text{CH}_3\text{C}(\text{O})\text{CH}(\text{OH})\text{-NCH}_3$ carbonolamine intermediate, which loses water to produce the imine product, was not detected by PTR-MS. These observations together are clear evidence for a methylglyoxal + methylamine reaction taking place on aerosol particles surfaces (and/or chamber walls), quantitatively producing a volatile imine that does not increase dry SMPS particle mass.

Two dark cloud events (C1 and C2) were triggered in the chamber by the addition of cold water vapor at $t = 5:30$ and $6:26$ h in experiment 2 (Figure 1; also $t = 6:12$ and $6:58$ h in experiment 1, Figure S1; $t = 6:20$ h in Figure S3). The dried aerosol particle albedo values are not changed significantly by these dark cloud events in experiments 1 or 2. However, when particles were sampled by CAPS without Nafion tube drying (expt 3, Figure S3), postcloud albedo increased by 0.02. This suggests that some light-absorbing species can be hydrolyzed

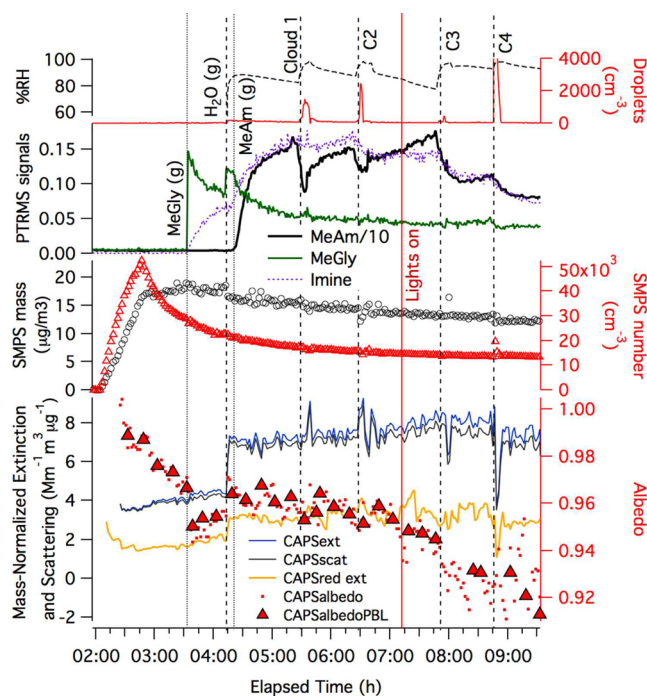


Figure 1. Ammonium sulfate seed/methylglyoxal/methylamine experiment 2 chamber RH and cloud droplet counts (top) shown with traces color-coded to axes. Middle: Dilution- and water-corrected PTR-MS traces are shown for gas-phase methylglyoxal ($m/z = 73$, green line), methylamine ($m/z = 32$, black line, signals divided by 10), and imine product ($m/z = 86$, purple dots). Dilution-corrected SMPS number density and particulate mass (assuming aerosol density = 1) are shown next, with an increasing number density indicating AS aerosol addition at the start of the experiment. Bottom: mass-normalized 2 min averaged CAPS extinction (blue line), scattering (black line), single-scattering albedo (red dots), and albedo values calculated from data immediately following instrument baseline (red triangles), all measured at 450 nm. CAPS extinction data measured at 630 nm (orange line) also shown. Additions of 0.8 ppm methylglyoxal gas and 1 ppm methylamine (vertical dotted lines), water vapor addition/four cloud events (dashed lines), and start of chamber illumination (red line) are labeled.

during cloud processing, but the hydrolysis products reform into brown carbon as the particles are rapidly dried in the sampling line. This reversible fading/browning process caused by wetting and drying can be termed “hydrochromism.”

In experiment 2 (Figure 1), the solar simulator lights were turned on at $t = 7:25$ h for two “photolytic” cloud events. For 20 min after the lights were turned on, little change is observed in aerosol single-scattering albedo. This lack of change is difficult to interpret. It may indicate that few light-absorbing products are present or that the light-absorbing products are not easily destroyed by photolysis or that light-absorbing products are photolyzed and then reformed as the particles are dried in the sampling line, an example of rapid photochromism.³⁴ However, starting at the first photolytic cloud event (C3) and continuing through C4, aerosol single-scattering albedo declines by 0.032 over the next 100 min while the aerosol mass remains nearly constant. It is clear from the lack of browning observed earlier that brown carbon formation here requires both photolysis and the presence of aqueous-phase droplets. The key species in this brown carbon formation event must therefore be a photolysis product, either formed directly in the aqueous phase or taken up after photolysis in the gas phase,

whose appearance triggers aqueous-phase production of small amounts of strongly light-absorbing species. This appears to be a type of autocatalytic photosensitization, where brown carbon photolyzes into radical species, which react with organic compounds present to form greater amounts of brown carbon. Identifying the chemical mechanism involved in this process is the subject of ongoing work.

Glycine Aerosol Seeds. Chamber experiment 4 (Figures 2 and S7) was conducted at $RH \geq 65\%$ with glycine aerosol. The

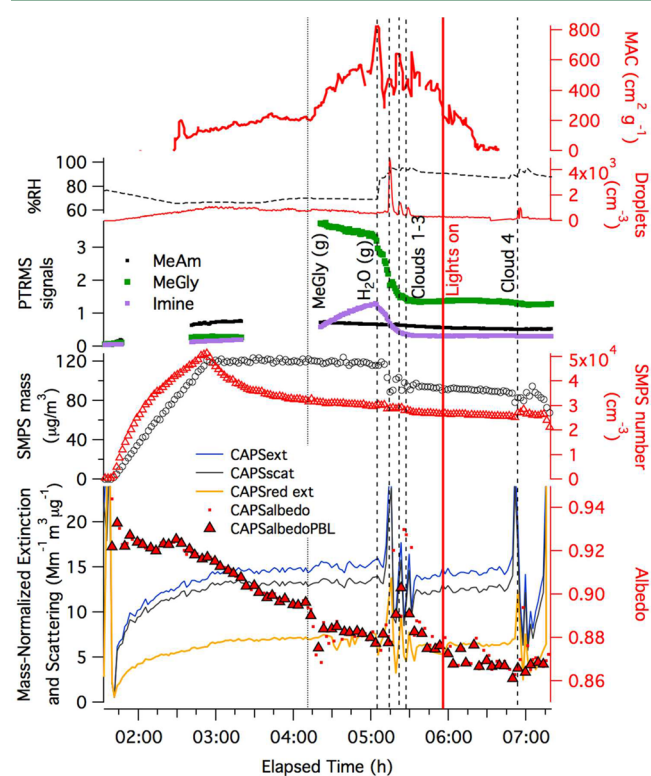


Figure 2. Glycine aerosol + methyl-glyoxal experiment 4 data summary. Top: MAC at 365 nm (thick red line) in PILS outflow. Chamber RH and cloud droplet counts are shown next with traces color-coded to axes. Middle: dilution- and water-corrected PTR-MS data points are shown for gas-phase methylglyoxal ($m/z = 73$, green), methylamine equilibrating from chamber walls ($m/z = 32$, black), and the imine product of methylglyoxal + methylamine wall reaction ($m/z = 86$, purple). Dilution-corrected SMPS number density and particulate mass (assuming aerosol density = 1) are shown next, with increasing number density indicating glycine aerosol addition at the start of the experiment. Bottom: mass-normalized 2 min averaged CAPS extinction (blue line), scattering (black line), single-scattering albedo (red dots), and postbaseline albedo values (red triangles), all measured at 450 nm. CAPS extinction data measured at 630 nm (orange line) also shown. Additions of 5.9 ppm methylglyoxal gas (dotted line), water vapor additions/cloud events (dashed lines), and start of chamber illumination (red line) are labeled.

addition of glycine aerosol particles ends at $t = 2:55$ h, at which point albedo = 0.92, clearly below the expected value for nonabsorbing aerosol after accounting for truncation and nonlinearity in the CAPS calibration. At this time, methylamine and methylglyoxal PTR-MS signals are elevated, even though these compounds have not been added to the chamber in this experiment. Moderate humidity levels in the chamber hydrolyze reaction products on the chamber walls from previous experiments, creating a steady-state background gas concen-

tration of methylglyoxal (1.0 ppm) and methylamine (0.4 ppm). This effect has been reported previously for glyoxal oligomers in chamber experiments.^{35,36} It appears that steady-state levels of gas-phase methylglyoxal, methylamine, imine product, or a related species may be causing browning of the glycine seed aerosol.

At $t = 4:10$ h, addition of gas-phase methylglyoxal causes a 7-fold increase in methylglyoxal concentrations and triggers a steady increase in the methylglyoxal–methylamine product imine signal at m/z 86. The large increase in methylglyoxal concentrations coincides with the onset of increasing aerosol mass absorption coefficients observed at 365 nm via PILS sampling, and with a drop of 0.02 in the aerosol albedo at 450 nm, occurring over a 4 min period. Increasing MAC and declining albedo both indicate aerosol browning. At the point of methylglyoxal addition, the glycine seed particles should be liquid,³⁷ since they were not dried prior to spraying into the humidified chamber. However, the rapid browning upon exposure to methylglyoxal is almost as fast as that observed on solid AS seed particles.

After the sudden drop in albedo upon methylglyoxal gas addition, over the next 40 min MAC increases, albedo decreases to 0.88, gas-phase methylglyoxal PTR-MS signals slowly decline as methylglyoxal is taken up by aerosol (and chamber walls), and m/z 86 signals increase as the imine produced by the methylglyoxal + methylamine reaction is released to the gas phase. All of these trends, consistent with aerosol browning, are interrupted by water vapor addition (at $t = 5:05$ h) and cloud events 1–3. Starting at this point, methylglyoxal and imine product are removed from the gas phase at increased rates, and albedo and MAC level off (with increased noise). The lack of browning observed during cloud processing is likely due to dilution of reactants by aerosol water uptake in the chamber, which remained above 86% RH for the rest of the experiment. However, after C3, the imaginary component of the index of refraction of the dried aerosol (calculated from CAPS 450 nm and SMPS data) quickly increases from 0.02 to 0.03 ± 0.009 (Figure S8). These were the most absorbing aerosols detected in any seeded experiment.

Between C3 and C4 (including when the lights come on at $t = 5:55$ h), further declines are measured in aerosol albedo (measured at 450 nm by CAPS-ssa), indicating continued browning, but aerosol absorbance (MAC measured at 365 nm in PILS outflow) starts to decline, especially after the lights come on. This decline in MAC is likely due to photolytic bleaching of brown carbon species.³⁸ However, since bleaching is not observed by CAPS in fully dried aerosol, it appears likely that thermochromism³⁴ is taking place, where photolytic products reform brown carbon species as the aqueous aerosol particles are rapidly dried in the CAPS sampling line. Unlike in experiment 2, no additional browning is observed after a photolytic cloud event (C4).

Methylammonium Sulfate Aerosol Seeds. Data from experiment 5, conducted above 70% RH on $(\text{CH}_3\text{NH}_3)_2\text{SO}_4$ seeds, is shown in Figures 3 and S9. In this experiment, the dried aerosol was probed by ABI since the efflorescence and deliquescence behavior of this aerosol seed is not known. The low bounce fraction (BF) of aerosol particles throughout the experiment (Figure S10) indicates that methylammonium sulfate aerosol particles remain liquid even at low RH. Interestingly, BF of the seed particles was ~ 0.3 at the beginning of the RH scan ($\sim 25\%$ RH), but due to particle stickiness and high number concentrations (~ 1000 – 2400 cm^{-3} of size

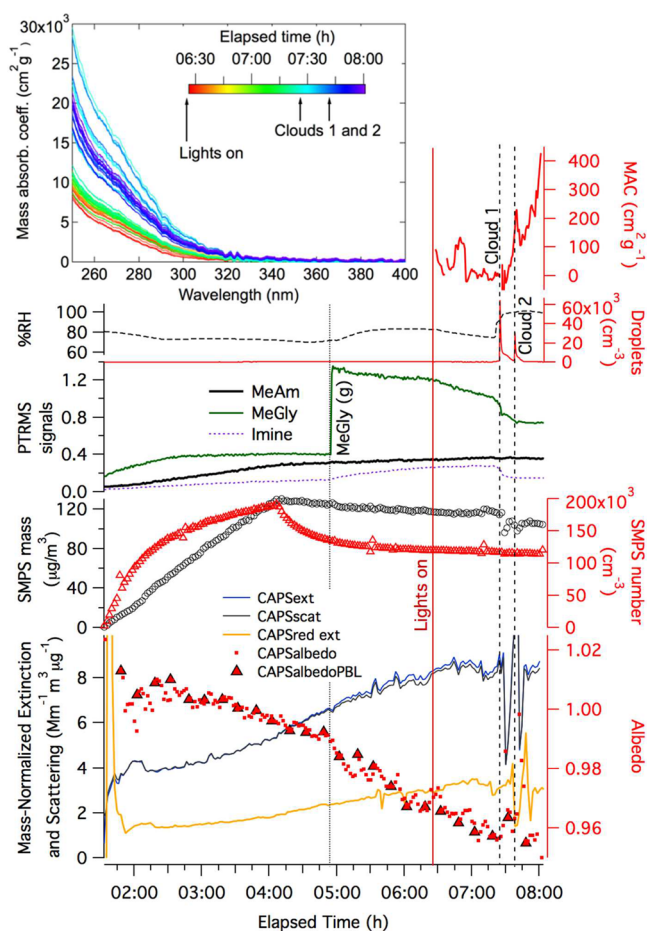


Figure 3. Methylammonium sulfate aerosol + methylglyoxal experiment 5 mass absorption coefficient at 365 nm of PILS outflow (top, red line) and time-dependent MAC spectra (top inset). Chamber RH and cloud droplet counts shown next. Middle: dilution- and water-corrected PTR-MS signals for gas-phase methylglyoxal ($m/z = 73$, green line), methylamine ($m/z = 32$, black line), and the imine product of methylglyoxal + methylamine reaction ($m/z = 86$, purple dots). Dilution-corrected SMPS number density and particulate mass (assuming aerosol density = 1) are shown next, with increasing number density indicating $(\text{CH}_3\text{NH}_3)_2\text{SO}_4$ aerosol addition until $t = 4$ h. Bottom: mass-normalized 2 min averaged CAPS extinction (blue line), scattering (black line), single-scattered albedo (red dots), and albedo values calculated from data immediately following instrument baseline (red triangles), all measured at 450 nm. CAPS extinction data measured at 630 nm (orange line) also shown. Additions of methylglyoxal gas (from 1.7 to 3.6 ppm, dotted line), solar simulator lights (red line), and water vapor additions/cloud events (dashed lines) are labeled.

selected particles), particles adhered to the impaction plate and decreased BF for subsequent particles, causing a downward trend in BF even at constant RH. Neither the addition of methylglyoxal to the gas phase, chamber illumination, nor cloud events increased BF beyond its initial value of ~ 0.3 . We can conclude that the $(\text{CH}_3\text{NH}_3)_2\text{SO}_4$ particles were near liquid and sticky at $\text{RH} < 30\%$ and fully liquid at $\text{RH} \geq 30\%$. By comparison, pure nebulized methylglyoxal particles' BF decreased from ~ 0.8 to 0.6 as RH increased from 10% to 70%, and BF dropped to zero at $\text{RH} \geq 76 \pm 3\%$ (see Supporting Information).

Methylglyoxal gas addition at $t = 4:55$ h increased its concentration from 1.0 to 3.6 ppm. Methylglyoxal addition

coincides with an accelerated decline in albedo, rather than a sudden drop as observed in previous experiments. An increased rate of release of the imine product into the gas phase is also observed by PTR-MS.

Single-scattering albedo at 450 nm continues its decline, perhaps due to thermochromism, through the onset of chamber illumination at $t = 6:25$ h and two photolytic cloud events (at $t = 7:25$ and $7:40$ h). Significantly, the first photolytic cloud event triggers a 30 min rise in mass absorption coefficients of the PILS outflow, a measurement that involves only partial drying of the aerosol. This is additional evidence that brown carbon species are formed in the aqueous phase in a process involving photolysis products at high RH. Production of brown carbon via this light-activated pathway is significantly faster than photolytic bleaching of the brown products.

No Seed Experiment. Data from experiment 6 where gas-phase methylglyoxal and methylamine were subjected to repeated cloud cycles in a seed-free chamber is shown in Figure S11. Methylglyoxal (2.7 ppm) and methylamine (1 ppm) were added to a dry chamber (RH < 1%). PTR-MS signals for methylamine reach a stable maximum within 7 min of addition, or about 4× faster than in experiments with humidified AS seed particles. In the 26 min after methylamine addition, methylglyoxal PTR-MS signals decline from 2.0 to 0.10 ppm in a pseudo-1st-order decay ($k' = 2.40 \times 10^{-3} \text{ s}^{-1}$, Figure S12), while imine product signals greatly increase, suggesting that methylamine reacts with methylglyoxal on the chamber walls. Before methylamine addition, methylglyoxal was lost to the walls with a first-order rate constant $k = 1.36 \times 10^{-4} \text{ s}^{-1}$. Methylamine addition thus appears to have catalyzed an increase in the methylglyoxal loss rate of $k' = 2.26 \times 10^{-3} \text{ s}^{-1}$. Since methylamine quickly reaches a steady-state concentration with $[\text{MeAm}] \gg [\text{MeGly}]$, if the reaction is first order with respect to methylglyoxal, as observed in aqueous-phase reactions with glyoxal,³⁹ then $k' = k[\text{MeAm}]$. Given $[\text{MeAm}] = (1 \pm 0.2) \text{ ppm} = (2.5 \pm 0.6) \times 10^{13} \text{ molecules cm}^{-3}$, the rate constant k for the methylamine-catalyzed methylglyoxal wall reaction is $(9 \pm 2) \times 10^{-17} \text{ cm}^3 \text{ molecule}^{-1} \text{ s}^{-1}$ at 294 K. A similar analysis of methylglyoxal decays in experiment 3 resulted in $k = (5.2 \pm 1.2) \times 10^{-17} \text{ cm}^3 \text{ molecule}^{-1} \text{ s}^{-1}$ at 288 K in the presence of methylamine and dry AS seeds. The activation energy of this reaction can therefore be estimated as $E_a = 64 \pm 37 \text{ kJ/mol}$, similar to aqueous-phase methylglyoxal + amino acid reactions where dehydration was the rate-limiting step.⁴⁰

Local supersaturation caused by expansion cooling of the water vapor jet produces water droplets that evaporate within a few seconds as they mix into the dry chamber. This process, which can be considered the briefest of cloud events, is seen at $t = 2$ h in the SMPS data in Figure S11 to produce a background of low-mass (small) aerosol particles consisting of either nonvolatile impurities from deionized water or methylglyoxal–methylamine aqueous-phase reaction products. The extinction measured at 450 nm for these particles, although near the detection limit of the CAPS instrument, is significantly greater than the scattering signals, resulting in albedo = 0.58 ± 0.05 , which is even lower than the albedo measured for 100 nm aerosol consisting of the black dye nigrosin (Figure S13). It is unlikely that trace nonvolatile impurities in deionized water would so be highly absorbing. Whatever their source, these highly absorbing aerosol species are not diluted by non-absorbing seed particle material, in contrast to experiments 1–5.

DISCUSSION

In published bulk-phase aqueous experiments on methylglyoxal mixtures with AS, ammonium nitrate, glycine, or methylamine, brown carbon production took days to reach completion in high-concentration solutions at pH 2–4.^{23,41} In this study, dry AS aerosol particles browned (as detected by CAPS at 450 nm) at rates limited by chamber mixing (<1 min), aqueous glycine aerosol browned within 4 min, and aqueous methylammonium sulfate aerosol browned continuously for a few hours when exposed to methylglyoxal vapor. A comparison between bulk and liquid aerosol browning rates, measured as mass absorption coefficients at 365 nm, is shown in Figure 4. Browning in

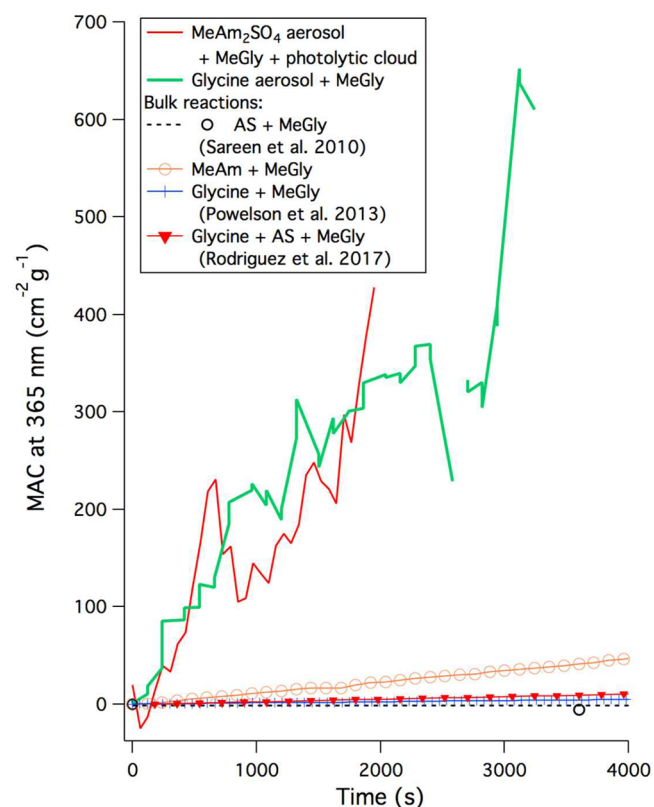


Figure 4. Comparison of time-dependent mass absorption coefficients measured at 365 nm during browning events in deliquesced aerosol in experiments 4 (glycine, green line) and 5 (methylammonium sulfate, red line), and in bulk aqueous phase experiments: 16 mM MeGly + 3.1 M AS (black dotted line and circles, ref 23); 0.25 M MeGly + 0.25 M methylamine (orange line and circles, ref 41); 0.125 M MeGly + 0.25 M glycine (blue line and + symbols, ref 41); 0.25 M MeGly + 0.25 M AS + 0.05 glycine (red line and triangles, ref 44).

deliquesced methylammonium sulfate aerosol after a photolytic cloud event is 13× faster than in a bulk aqueous-phase experiment at 0.25 M, and browning in deliquesced glycine aerosol upon exposure to methylglyoxal gas is over 500× faster than three bulk aqueous-phase experiments with glycine or AS. All of these results suggest that aqueous- and aerosol-phase reactions involving methylglyoxal can form brown carbon at rates that are orders of magnitude faster than those in bulk solution. It is unlikely that differences in concentration can explain all of this acceleration, since the high aqueous-phase concentrations used in typical bulk browning experiments are meant to simulate the aerosol phase. Browning in aldehyde–amine mixtures is known to accelerate at basic

pH,⁴² but in all seeded experiments browning was observed on aerosol expected to be slightly acidic.

Instead, fast aerosol browning reactions are likely taking place at aerosol surfaces. The surface-to-volume ratio of a population of submicron aerosol is $\sim 10^5 \times$ larger than that of a typical bulk aqueous experiment. In room-temperature solutions at equilibrium, methylglyoxal's reactive aldehyde functional group is 99.7% hydrated,⁴³ and the hydrate is much less photolytically and chemically active. At a surface or interface, on the other hand, incomplete hydration shells will shift the equilibrium away from the hydrate, allowing some reactive aldehyde functional groups to reappear. In addition, methylglyoxal and its reaction products are surface active,²³ reducing surface tension and preferentially occupying positions on the aqueous surface rather than in the bulk.

In all experiments, growth of the dried aerosol was less than $1 \mu\text{g}/\text{m}^3$, suggesting that the small amount of material formed by methylglyoxal uptake reactions was extremely light absorbing, such that declines in single-scattering albedo could be detected even when aerosol growth was not. This conclusion is consistent with the small amount of highly absorbing aerosol (albedo ~ 0.6 , mass $< 0.6 \mu\text{g}/\text{m}^3$) detected after cloud processing of methylglyoxal and methylamine gas in a seed-free chamber. Under these conditions, aqueous-phase brown carbon products did not get diluted with nonabsorbing seed particle materials.

At low RH, reactive methylglyoxal uptake to aerosol surfaces may be catalyzed by trace amounts of adsorbed water, slowing only when reaction sites on the solid surface become saturated with adsorbed products or other species, or when the catalytic surface-adsorbed water itself is lost. The uptake of methylglyoxal on dry AS aerosol is likely analogous to the reactive uptake of glyoxal observed on dry glycine aerosol particles;⁴⁵ however, with glyoxal clear increases in aerosol mass are observed.

The majority of methylglyoxal uptake and browning of dry AS seed aerosol was reversed upon humidification. At high RH, previously formed brown carbon products on the aerosol surface can be hydrolyzed back to the original reactants, which may then re-equilibrate with the gas phase. Furthermore, dilution of reactants by particle-phase water will slow aqueous-phase browning reactions even as scavenging of water-soluble gases increases. Reduced oligomer formation, especially by condensation reactions, has been observed at high RH in SOA formed by isoprene + OH chemistry.⁴⁶ Since many light-absorbing species are produced from methylglyoxal by aldol condensation reactions,^{23,43} a slowdown in condensation reactions may contribute to the slower browning observed at high RH in the dark.

Several types of brown carbon, including methylglyoxal/AS mixtures, are readily photobleached in bulk phase experiments.^{38,47} In this work, brown carbon/deliquesced glycine aerosol particles were observed to fade in one experiment when photolyzed at high RH and sampled at 40% RH. However, no fading was observed when the same particles were simultaneously sampled dry, and no fading was observed in any other brown carbon experiment involving dry sampling, suggesting that even when brown carbon is photolyzed in aqueous aerosol, light-absorbing species can reform from the fragments when the aerosol particle is dried. A similar, slower thermochromic process in pyruvic acid solutions was attributed to photo-induced hydration of C=C bonds, followed by rebrowning *via*

dehydration.³⁴ The drying of an aerosol particle would be expected to greatly accelerate such dehydration reactions.

Significantly, photolytic cloud processing in the presence of methylglyoxal and methylamine was observed to increase brown carbon formation on both AS and methylammonium sulfate seed particles, regardless of whether particles were sampled wet or dry. Neither cloud processing nor photolysis increased brown carbon formation separately, which indicates that an aqueous and multiphase process involving photolysis products is capable of rapid brown carbon formation, even outpacing the direct photolytic loss of brown carbon (as measured at 450 nm). This surprising phenomenon must be an autocatalytic type of photosensitization. Normally, photosensitization describes a process where light-absorbing molecules in the aqueous phase are photolyzed and form relatively long-lived triplet radical species, which then oxidize other molecules and contribute to increased SOA mass.⁴⁸ Here, brown carbon photolysis in aqueous cloud droplets and aqueous aerosol particles produces radical species, which then combine with other molecules to produce more brown carbon in the cloud aftermath, contributing to increasing light absorption by aerosol particles. Brown carbon production from triplet species has been reported in aqueous syringol SOA.⁴⁹ Clearly, chemical characterization of the mechanisms involved is needed so that the importance of autocatalytic photosensitization can be evaluated in models.

In this study, methylglyoxal and methylamine were present at low parts per million quantities, whereas in the atmosphere only low- or sub-parts-per-billion quantities would be expected outside of polluted environments. Changes in aerosol single-scattering albedo caused by uptake of low-parts-per-billion quantities of methylglyoxal would likely fall below the detection limits of CAPS-ssa and PILS-waveguide spectrometers. Even at the low parts per million methylglyoxal concentrations used in this work, it was difficult to detect the production of SOA mass by SMPS, consistent with earlier studies on AS and acidified AS aerosol, where aerosol volumes increased by $< 5 \mu\text{m}^3/\text{cm}^3$ upon exposure to 1 ppm methylglyoxal.³⁶ While brown carbon and SOA formation *via* methylglyoxal uptake and subsequent photolytic cloud processing may thus be expected to have a negligible effect on the albedo and mass of atmospheric aerosol, due to lower atmospheric precursor concentrations, if additional light-absorbing species can autocatalyze the production of brown carbon via photosensitization in the presence of AS and amine-containing aerosol, this may represent a new, significant source of brown carbon in the atmosphere. We note that primary brown carbon and HULIS are widespread in atmospheric aerosol and that a fraction of BrC from biomass burning is resistant to photobleaching.⁵⁰ It would be worth testing aerosolized extracts of these materials for autocatalytic browning behavior.

■ ASSOCIATED CONTENT

📄 Supporting Information

The Supporting Information is available free of charge on the ACS Publications website at DOI: 10.1021/acs.est.7b00159.

Pressure, temperature, and PTR-MS data for other *m/z* ratios for each chamber experiment; a sample CAPS calibration; SMPS pre- and postcloud aerosol size distributions; bounce fraction data for methylamine sulfate and three other particle types; graphs of time-dependent imaginary components of the index of

refraction; data from an AS + cloud control experiment; discussion of albedo baselines and excursions measured between baseline events; aerosol density and phase; aerosol and chamber cloud lifetimes; and aerosol bounce measurements (PDF)

AUTHOR INFORMATION

Corresponding Author

*Phone: (619) 260-6882. Fax: (619) 260-2211. E-mail: ddehaan@sandiego.edu.

ORCID

David O. De Haan: 0000-0003-4559-2284

Present Address

[†]L.C.: PM_TEN s.r.l., via Dodecaneso 33, 16146 Genova, Italy.

Notes

The authors declare no competing financial interest.

ACKNOWLEDGMENTS

This work was funded by NSF grants AGS-1523178 and NSF AGS-1555003. L.N.H. was funded by the Barbara Stokes Dewey Foundation and Research Corporation (CCSA 22473). CNRS-INSU is gratefully acknowledged for supporting CESAM as an open facility through the National Instrument label.

REFERENCES

- (1) Pankow, J. F. An absorption model of gas/particle partitioning of organic compounds in the atmosphere. *Atmos. Environ.* **1994**, *28* (2), 185–188.
- (2) Lee, S.; Jang, M.; Kamens, R. M. SOA formation from the photooxidation of α -pinene in the presence of freshly emitted diesel soot exhaust. *Atmos. Environ.* **2004**, *38*, 2597–2605.
- (3) Pankow, J. F.; Seinfeld, J. H.; Asher, W. E.; Erdakos, G. B. Modeling the formation of secondary organic aerosol. 1. Application of theoretical principles to measurements obtained in the α -pinene/, β -pinene/, sabinene/, Δ^3 -carene/, and cyclohexene/ozone systems. *Environ. Sci. Technol.* **2001**, *35* (6), 1164–1172.
- (4) Wang, X.; Gao, S.; Yang, X.; Chen, H.; Chen, J.; Zhuang, G.; Surratt, J. D.; Chan, M. N.; Seinfeld, J. H. Evidence for high molecular weight nitrogen-containing organic salts in urban aerosols. *Environ. Sci. Technol.* **2010**, *44* (12), 4441–4446.
- (5) Ramanathan, V.; Li, F.; Ramana, M. V.; Praveen, P. S.; Kim, D.; Corrigan, C. E.; Nguyen, H.; Stone, E. A.; Schauer, J. J.; Carmichael, G. R.; Adhikary, B.; Yoon, S. C. Atmospheric brown clouds: hemispherical and regional variations in long-range transport, absorption, and radiative forcing. *J. Geophys. Res.* **2007**, *112* (D22), D22S21/1–D22S21/26.
- (6) Baduel, C.; Voisin, D.; Jaffrezo, J.-L. Seasonal variations of concentrations and optical properties of water soluble HULIS collected in urban environments. *Atmos. Chem. Phys.* **2010**, *10*, 4085–4095.
- (7) Fan, X.; Song, J.; Peng, P. Comparative study for separation of atmospheric humic-like substance (HULIS) by ENVI-18, HLB, XAD-8 and DEAE sorbents: Elemental composition, FT-IR, ¹H NMR and off-line thermochemolysis with tetramethylammonium hydroxide (TMAH). *Chemosphere* **2013**, *93*, 1710–1719.
- (8) Fors, E. O.; Rissler, J.; Massling, A.; Svenningsson, B.; Andreae, M. O.; Dusek, U.; Frank, G. P.; Hoffer, A.; Bilde, M.; Kiss, G.; Janitsek, S.; Henning, S.; Facchini, M. C.; Decesari, S.; Swietlicki, E. Hygroscopic properties of Amazonian biomass burning and European background HULIS and investigation of their effects on surface tension with two models linking H-TDMA to CCNC data. *Atmos. Chem. Phys.* **2010**, *10*, 5625–5639.
- (9) Guilhermet, J.; Preunkert, S.; Voisin, D.; Baduel, C.; Legrand, M. Major 20th century changes of water-soluble humic-like substances

(HULISWS) aerosol over Europe inferred from Alpine ice cores. *J. Geophys. Res.: Atmos.* **2013**, *118* (9), 3869–3878.

(10) Hoffer, A.; Gelencser, A.; Guyon, P.; Kiss, G.; Schmid, O.; Frank, G. P.; Artaxo, P.; Andreae, M. O. Optical properties of humic-like substances (HULIS) in biomass-burning aerosols. *Atmos. Chem. Phys.* **2006**, *6*, 3563–3570.

(11) Kristensen, T. B.; Du, L.; Nguyen, Q. T.; Nøjgaard, J. K.; Bender Koch, C.; Faurskov Nielsen, O.; Hallar, A. G.; Lowenthal, D. H.; Nekat, B.; van Pinxteren, D.; Herrmann, H.; Glasius, M.; Kjaergaard, H. G.; Bilde, M. Chemical properties of HULIS from three different environments. *J. Atmos. Chem.* **2015**, *72*, 65–80.

(12) Hecobian, A.; Zhang, X.; Zheng, M.; Frank, N.; Edgerton, E. S.; Weber, R. J. Water-soluble organic aerosol material and the light-absorption characteristics of aqueous extracts measured over the southeastern United States. *Atmos. Chem. Phys.* **2010**, *10*, 5965–5977.

(13) Öktem, B.; Tolocka, M. P.; Johnston, M. V. On-line analysis of organic components in fine and ultrafine particles by photoionization aerosol mass spectrometry. *Anal. Chem.* **2004**, *76* (2), 253–261.

(14) Bones, D. L.; Henricksen, D. K.; Mang, S. A.; Gonsior, M.; Bateman, A. P.; Nguyen, T. B.; Cooper, W. J.; Nizkorodov, S. A. Appearance of strong absorbers and fluorophores in limonene-O₃ secondary organic aerosol due to NH₄⁺-mediated chemical aging over long time scales. *J. Geophys. Res.* **2010**, *115* (D5), D05203/1–D05203/14.

(15) Nguyen, T. B.; Lee, P. B.; Updyke, K. M.; Bones, D. L.; Laskin, J.; Laskin, A.; Nizkorodov, S. A. Formation of nitrogen- and sulfur-containing light-absorbing compounds accelerated by evaporation of water from secondary organic aerosols. *J. Geophys. Res.* **2012**, *117*, D01207.

(16) Laskin, A.; Laskin, J.; Nizkorodov, S. A. Chemistry of Atmospheric Brown Carbon. *Chem. Rev.* **2015**, *115*, 4335–4382.

(17) Lin, P.; Laskin, J.; Nizkorodov, S. A.; Laskin, A. Revealing Brown Carbon Chromophores Produced in Reactions of Methylglyoxal with Ammonium Sulfate. *Environ. Sci. Technol.* **2015**, *49* (24), 14257–14266.

(18) Ervens, B.; Turpin, B. J.; Weber, R. J. Secondary organic aerosol formation in cloud droplets and aqueous particles (aqSOA): A review of laboratory, field and model studies. *Atmos. Chem. Phys.* **2011**, *11*, 11069–11102.

(19) Hawkins, L. N.; Lemire, A. N.; Galloway, M. M.; Corrigan, A. L.; Turley, J. J.; Espelien, B. M.; De Haan, D. O. Maillard Chemistry in Clouds and Aqueous Aerosol As a Source of Atmospheric Humic-Like Substances. *Environ. Sci. Technol.* **2016**, *50*, 7443–7452.

(20) De Haan, D. O.; Corrigan, A. L.; Smith, K. W.; Stroik, D. R.; Turley, J. T.; Lee, F. E.; Tolbert, M. A.; Jimenez, J. L.; Cordova, K. E.; Ferrell, G. R. Secondary Organic Aerosol-Forming Reactions of Glyoxal with Amino Acids. *Environ. Sci. Technol.* **2009**, *43* (8), 2818–2824.

(21) Noziere, B.; Dziedzic, P.; Cordova, A. Formation of secondary light-absorbing “fulvic-like” oligomers: a common process in aqueous and ionic atmospheric particles? *Geophys. Res. Lett.* **2007**, *34*, L21812.

(22) Noziere, B.; Cordova, A. A kinetic and mechanistic study of the amino acid catalyzed aldol condensation of acetaldehyde in aqueous and salt solutions. *J. Phys. Chem. A* **2008**, *112* (13), 2827–2837.

(23) Sareen, N.; Schwier, A. N.; Shapiro, E. L.; Mitroo, D.; McNeill, V. F. Secondary organic material formed by methylglyoxal in aqueous aerosol mimics. *Atmos. Chem. Phys.* **2010**, *10*, 997–1016.

(24) Shapiro, E. L.; Szprengiel, J.; Sareen, N.; Jen, C. N.; Giordano, M. R.; McNeill, V. F. Light-absorbing secondary organic material formed by glyoxal in aqueous aerosol mimics. *Atmos. Chem. Phys.* **2009**, *9*, 2289–2300.

(25) Wang, J.; Doussin, J. F.; Perrier, S.; Perraudin, E.; Katrib, Y.; Pangui, E.; Picquet-Varrault, B. Design of a new multi-phase experimental simulation chamber for atmospheric photo-smog, aerosol and cloud chemistry research. *Atmos. Meas. Tech.* **2011**, *4*, 2465–2494.

(26) Onasch, T. B.; Massoli, P.; Keegan, P. L.; Hills, F. B.; Bacon, F. W.; Freedman, A. Single scattering albedo monitor for airborne particulates. *Aerosol Sci. Technol.* **2015**, *49* (4), 267–279.

- (27) McGarragh, G. *mie_single.pro*; Earth Observation Data Group, University of Oxford Department of Physics: Oxford, U.K., 2016. http://eodg.atm.ox.ac.uk/MIE/mie_single.html.
- (28) *Eurochamp-2: Integration of European Simulation Chambers for Investigating Atmospheric Processes*; CEAM: Valencia, Spain, 2010. http://www.eurochamp.org/data_base/index.html.
- (29) Pajunoja, A.; Lambe, A. T.; Hakala, J.; Rastak, N.; Cummings, M. J.; Brogan, J. F.; Hao, L.; Paramonov, M.; Hong, J.; Prisle, N. L.; Malila, J.; Romakkaniemi, S.; Lehtinen, K. E. J.; Laaksonen, A.; Kulmala, M.; Massoli, P.; Onasch, T. B.; Donahue, N. M.; Riipinen, I.; Davidovits, P.; Worsnop, D. R.; Petäjä, T.; Virtanen, A. Adsorptive uptake of water by semisolid secondary organic aerosols. *Geophys. Res. Lett.* **2015**, *42* (8), 3063–3068.
- (30) Zhang, X.; Lin, Y.-H.; Surratt, J. D.; Zotter, P.; Prévôt, A. S. H.; Weber, R. J. Light-absorbing soluble organic aerosol in Los Angeles and Atlanta: A contrast in secondary organic aerosol. *Geophys. Res. Lett.* **2011**, *38* (21), L21810.
- (31) Zhang, X.; Lin, Y.-H.; Surratt, J. D.; Weber, R. J. Sources, Composition and Absorption Ångström Exponent of Light-absorbing Organic Components in Aerosol Extracts from the Los Angeles Basin. *Environ. Sci. Technol.* **2013**, *47* (8), 3685–3693.
- (32) Denjean, C.; Formenti, P.; Picquet-Varrault, B.; Katrib, Y.; Pangui, E.; Zapf, P.; Doussin, J. F. A new experimental approach to study the hygroscopic and optical properties of aerosols: application to ammonium sulfate particles. *Atmos. Meas. Tech.* **2014**, *7* (1), 183–197.
- (33) de Gouw, J. A.; Goldan, P. D.; Warneke, C.; Kuster, W. C.; Roberts, J. M.; Marchewka, M.; Bertman, S. B.; Pszenny, A. A. P.; Keene, W. C. Validation of proton transfer reaction-mass spectrometry (PTR-MS) measurements of gas-phase organic compounds in the atmosphere during the New England Air Quality Study (NEAQS) in 2002. *J. Geophys. Res.: Atmos.* **2003**, *108* (D21), DOI: [10.1029/2003JD003863](https://doi.org/10.1029/2003JD003863).
- (34) Rincón, A. G.; Guzmán, M. I.; Hoffmann, M. R.; Colussi, A. J. Thermochromism of model organic aerosol matter. *J. Phys. Chem. Lett.* **2010**, *1*, 368–373.
- (35) Liggio, J.; Li, S.-M.; McLaren, R. Reactive uptake of glyoxal by particulate matter. *J. Geophys. Res.* **2005**, *110*, D10304.
- (36) Kroll, J. H.; Ng, N. L.; Murphy, S. M.; Varutbangkul, V.; Flagan, R. C.; Seinfeld, J. H. Chamber studies of secondary organic aerosol growth by reactive uptake of simple carbonyl compounds. *J. Geophys. Res.* **2005**, *110*, D23207.
- (37) Chan, M. N.; Choi, M. Y.; Ng, N. L.; Chan, C. K. Hygroscopicity of water-soluble organic compounds in atmospheric aerosols: amino acids and biomass derived organic species. *Environ. Sci. Technol.* **2005**, *39* (6), 1555–1562.
- (38) Lee, H. J.; Aiona, P. K.; Laskin, A.; Nizkorodov, S. A. Effect of solar radiation on the optical properties and molecular composition of laboratory proxies of atmospheric brown carbon. *Environ. Sci. Technol.* **2014**, *48* (17), 10217–10226.
- (39) De Haan, D. O.; Tolbert, M. A.; Jimenez, J. L. Atmospheric condensed-phase reactions of glyoxal with methylamine. *Geophys. Res. Lett.* **2009**, *36*, L11819.
- (40) Sedehi, N.; Takano, H.; Blasic, V. A.; Sullivan, K. A.; De Haan, D. O. Temperature- and pH-dependent aqueous-phase kinetics of the reactions of glyoxal and methylglyoxal with atmospheric amines and ammonium sulfate. *Atmos. Environ.* **2013**, *77*, 656–663.
- (41) Powelson, M. H.; Espelien, B. M.; Hawkins, L. N.; Galloway, M. M.; De Haan, D. O. Brown carbon formation by aqueous-phase aldehyde reactions with amines and ammonium sulfate. *Environ. Sci. Technol.* **2014**, *48* (2), 985–993.
- (42) Davidek, T.; Velisek, J.; Davidek, J.; Pech, P. Amino acids derived 1,3-disubstituted imidazoles in nonenzymatic browning reactions. *Sbornik Vysoke Skoly Chemicko-Technologicke v Praze, E: Potraviny* **1991**, *62*, 165–182.
- (43) Krizner, H. E.; De Haan, D. O.; Kua, J. Thermodynamics and kinetics of methylglyoxal dimer formation: A computational study. *J. Phys. Chem. A* **2009**, *113* (25), 6994–7001.
- (44) Rodriguez, A. A.; de Loera, A.; Powelson, M. H.; Galloway, M. M.; De Haan, D. O. Formaldehyde and acetaldehyde increase aqueous-phase production of imidazoles in methylglyoxal - amine mixtures: Quantifying a secondary organic aerosol formation mechanism. *Environ. Sci. Technol. Lett.* **2017**, in press. DOI: [10.1021/acs.estlett.7b00129](https://doi.org/10.1021/acs.estlett.7b00129).
- (45) Loeffler, K. W.; Koehler, C. A.; Paul, N. M.; De Haan, D. O. Oligomer formation in evaporating aqueous glyoxal and methyl glyoxal solutions. *Environ. Sci. Technol.* **2006**, *40* (20), 6318–6323.
- (46) Nguyen, T. B.; Roach, P. J.; Laskin, J.; Laskin, A.; Nizkorodov, S. A. Effect of humidity on the composition of isoprene photooxidation secondary organic aerosol. *Atmos. Chem. Phys.* **2011**, *11* (14), 6931–6944.
- (47) Zhao, R.; Lee, A. K. Y.; Huang, L.; Li, X.; Yang, F.; Abbatt, J. P. D. Photochemical processing of aqueous atmospheric brown carbon. *Atmos. Chem. Phys.* **2015**, *15* (11), 6087–6100.
- (48) Monge, M. E.; Rosenørn, T.; Favez, O.; Müller, M.; Adler, G.; Abo Rizeq, A.; Rudich, Y.; Herrmann, H.; George, C.; D'Anna, B. Alternative pathway for atmospheric particles growth. *Proc. Natl. Acad. Sci. U. S. A.* **2012**, *109* (18), 6840–6844.
- (49) Yu, L.; Smith, J.; Laskin, A.; Anastasio, C.; Laskin, J.; Zhang, Q. Chemical characterization of SOA formed from aqueous-phase reactions of phenols with the triplet excited state of carbonyl and hydroxyl radical. *Atmos. Chem. Phys.* **2014**, *14* (24), 13801–13816.
- (50) Forrister, H.; Liu, J.; Scheuer, E.; Dibb, J.; Ziemba, L.; Thornhill, K. L.; Anderson, B.; Diskin, G.; Perring, A. E.; Schwarz, J. P.; Campuzano-Jost, P.; Day, D. A.; Palm, B. B.; Jimenez, J. L.; Nenes, A.; Weber, R. J. Evolution of brown carbon in wildfire plumes. *Geophys. Res. Lett.* **2015**, *42* (11), 4623–4630.